Raman spectroscopy predicts the link between claw keratin and bone collagen structure in a rodent model of oestrogen deficiency

Caraher, M. C., Sophocleous, S., Beattie, J. R., O'Driscoll, O., Cummins, N. M., Brennan, O., O'Brien, F. J., Bell, S. E. J., Towler, M., Ralston, S. H., & Idris, A. I. (2018). Raman spectroscopy predicts the link between claw keratin and bone collagen structure in a rodent model of oestrogen deficiency. *Biochimica et Biophysica Acta - Molecular Basis of Disease*, *1864*(2), 398-406. https://doi.org/10.1016/j.bbadis.2017.10.020

Published in:
Biochimica et Biophysica Acta - Molecular Basis of Disease

Document Version:
Peer reviewed version

Queen's University Belfast - Research Portal:
Link to publication record in Queen's University Belfast Research Portal

Raman spectroscopy predicts the link between claw keratin and bone collagen structure in a mouse model of oestrogen deficiency.

AUTHORS: M. Clare Caraher[1,2], Antonia Sophocleous[3,6], J. Renwick Beattie[5], Olive O'Driscoll[6], Niamh M. Cummins[7], Orlaith Brennan[8,9,10], Fergal J. O'Brien[8,9,10], Steven E. J. Bell[2], Mark Towler[11], Stuart H. Ralston[6], Aymen I. Idris[12]

AFFILIATIONS: [1]ICON plc, South County Business Park, Leopardstown, Dublin, IRELAND [2] School of Chemistry and Chemical Engineering, Queen's University Belfast, Stranmillis Road, Belfast, UK. [3]Department of Life Sciences, European University Cyprus, Nicosia, Cyprus. [4] J Renwick Beattie Consulting, Causeway Enterprise Agency, Ballycastle, UK. [5]AventaMed, Rubicon Centre, Rossa Avenue, Bishopstown, Cork, Ireland. [6]Rheumatology and Bone Diseases Unit, Centre for Genomic and Experimental Medicine, MRC Institute of Genetics and Molecular Medicine, Western General Hospital, University of Edinburgh, UK. [7]Centre for Interventions in Infection, Inflammation and Immunity, Graduate Entry Medical School, University of Limerick, Ireland. [8]Tissue Engineering Research Group, Department of Anatomy, Royal College of Surgeons in Ireland, Dublin, Ireland. [9]Trinity Centre for Bioengineering, Trinity College, Dublin, Ireland. [10]Advanced Materials and Bio-Engineering Research Centre (AMBER), RCSI & TCD, Dublin, Ireland. [11] Department of Mechanical and Industrial Engineering, Ryerson University, Toronto, ON, Canada. [12]Department of Oncology and Metabolism, Medical School, University of Sheffield, Beech Hill Road, Sheffield, U.K.

RUNNING TITLE: Raman spectroscopy predicts bone loss.

KEYWORDS: Raman, bone, collagen, claw, osteoporosis, age, microCT.

CORRESPONDENCE TO: Dr J. R. Beattie, J Renwick Beattie Consulting, Causeway Enterprise Agency, Ballycastle, UK. Email: rene@jrenwickbeattie.com

and

Dr A. I. Idris. Department of Oncology and Metabolism, Beech Hill Road, Sheffield, S10 2RX, UK. E-mail: aymen.idris@sheffield.ac.uk.

AUTHOR EMAILS: M. Clare Caraher (clarecaraher@gmail.com), Antonia Sophocleous (a.sophocleous@euc.ac.cy), J. Renwick Beattie (rene@jrenwickbeattie.com), Olive O'Driscoll (email:olive.odriscoll@aventamed.com), Niamh M. Cummins (email: niamh.cummins@ul.ie),

Orlaith Brennan (email:OBrennan1@rcsi.ie), Fergal J. O'Brien (email: fjobrien@rcsi.ie), Steven E. J. Bell (email:s.bell@qub.ac.uk), Mark Towler (mark.r.towler@gmail.com), Stuart H. Ralston (stuart.ralston@ed.ac.uk), Aymen I. Idris (aymen.idris@sheffield.ac.uk).

Abstract

Osteoporosis is a common disease characterised by reduced bone mass and an increased risk of fragility fractures. Low bone mineral density is known to significantly increase the risk of osteoporotic fractures, however, the majority of non-traumatic fractures occur in individuals with a bone mineral density too high to be classified as osteoporotic. Therefore, there is an urgent need to investigate aspects of bone health, other than bone mass, that can predict the risk of fracture. Here, we successfully predicted association between bone collagen and nail keratin in relation to bone loss due to oestrogen deficiency using Raman spectroscopy. Raman signal signature successfully discriminated between ovariectomised rats and their sham controls with a high degree of accuracy for the bone (sensitivity 89%, specificity 91%) and claw tissue (sensitivity 89%, specificity 82%). When tested in an independent set of claw samples the classifier gave 92% sensitivity and 85% specificity. Comparison of the spectral changes occurring in the bone tissue with the changes occurring in the keratin showed a number of common features that could be attributed to common changes in the structure of bone collagen and claw keratin. This study established a direct link between the structure of keratin in the claw and collagen in the bone, mediated by the changes induced by oestrogen deficiency.

Introduction

Postmenopausal osteoporosis is a common disease characterised by reduced bone mass and an increased risk of fragility fractures which increases dramatically in incidence with age [1]. The risk of osteoporosis is determined by a balance between levels of peak bone mass attained during skeletal growth and the amount of bone that is lost later on in life [2–5]. At menopause, declining oestrogen levels trigger an increase in bone remodelling with uncoupling of osteoclastic bone resorption from osteoblastic bone formation [6]. Evidence from rodent and nonhuman primate studies indicates that enhanced bone remodelling associated with deficiency in sex hormone leads to bone loss and increases risk of osteoporotic fractures [7–10].

The majority of osteoporotic fractures occur in patients with low bone mineral density (BMD), as assessed by Dual energy X-ray Absorptiometry (DXA) [11–13]. However, there is overlap in BMD between individuals with recurrent fractures and those who have not, inferring that low BMD is not the only cause of fragile bones [10,14]. Degree of mineralization is another standard by which osteoporosis is diagnosed, however it is often unreliable in detecting bone fragility. This is mainly due to its inability to take into account, amongst other factors [15], changes in the bone matrix protein, namely collagen. Studies have shown that collagen in osteotropic patients exhibits a different structure to normal collagen [16,17], and have found a correlation between these structural changes in collagen and bone fracture [18,19].

Raman spectroscopy is a sensitive and non-invasive optical technique in which the transfer of energy from light to matter gives ‘fingerprint’ information of a sample’s chemical composition and physical state. The technique is commonly used in chemical analysis e.g. in forensic, and pharmaceutical science, however more recently it has been identified as a potential tool for evaluating bone. Using Raman spectroscopy, a comparison study of iliac crest biopsies and femoral head samples revealed that osteoporotic women with fractures had a greater carbonate/phosphate ratio in cortical bone and a higher carbonate/amide I ratio in femoral

trabecular bone when compared to healthy women [20]. Other studies by Pillay *et al*, Towler *et al.* and Moran *et al.* used Raman spectroscopy to demonstrate that nails from osteoporotic patients had lower disulphide bonding compared to healthy controls [21–23]. A subsequent clinical study on 633 nail donors showed that Raman analysis of the fingernails was capable of discriminating between donors who had and who had not suffered a fragility fracture[24]. A prospective study based on archived nails with 20 years of follow up information demonstrated that the Raman based approach is capable of predicting those at high risk of fracture up to 13 years in advance of the onset of the fracture[25]. Detailed spectroscopic investigation revealed that the structural integrity of the keratin in the nail was different between the groups, with the fracture group exhibiting a more disordered protein structure than the non-fracture group [26]. Together, these findings led to the hypothesis that changes in composition and structure of keratin (nail) in osteoporotic models may act as a surrogate marker of systemic processes that affect the structural proteins in the bone matrix (collagen). In this study, we further tested this hypothesis by comparing the changes in claw keratin Raman spectra with the changes in the proteins, chemical composition and architectural changes due to oestrogen deficiency in rats.

Materials and Methods

Animal experiments

All animal experiments were approved by the Animal Welfare and Ethical Review Body of the University of Edinburgh (Scotland, UK) and conducted in accordance with the UK Animals (Scientific Procedures) Act 1986. Animals were housed under standard conditions of temperature (25 ± 1°C) and relative humidity (60 ± 10%) on 12 hours light/dark cycle with *ad libitum* access to standard pellet diet and tap water.

Ovariectomy and hormone replacement

Ovariectomy or sham ovariectomy was performed in 12 weeks old Sprague-Dawley rats as previously described [27]. The experiment terminated on day 77 and bone mineral density was measured at the tibial metaphysis by micro computed tomography (microCT).

Animal study design

Sprague-Dawley study design and treatments

The Sprague-Dawley study was designed and carried out at the University of Edinburgh (Scotland, UK). The rats were randomly assigned to 1 of 3 groups: ovariectomy (OVX, n=10), sham-operated (n=10) or naïve group (n=9). All rats were sacrificed at 23 weeks of age and bone samples (right femur) were collected and stored at -20°C. Claw samples (right and left claw) were collected and stored at 4°C.

Wistar study design and treatments

The Wistar study was developed by the Royal College of Surgeons in Ireland (RCSI, Dublin, Ireland). This study details the analysis of the claw samples using Raman spectroscopy carried out at Queen's University Belfast. Under the terms of agreement bone samples were not made available. A total of 65 retired breeder Wistar rats were randomly assigned to 1 of 11 groups including those that underwent surgical intervention and age-matched controls (Table 1). After completion of surgical intervention, the claw samples (right front and hind claws and left front and hind claws – 4 claws from each specimen) were collected and stored at 4°C.

Micro-computed tomography

Bone architecture was assessed using Micro-computed tomography (microCT) at the University of Edinburgh (Scotland, UK). Trabecular and cortical bone parameters were analysed as previously describe by Campbell & Sophocleous [28], using a Skyscan 1172 instrument (Brucker, Belgium) set at 70kV and 142μA and at a resolution of 10μm. Images were then reconstructed by the Skyscan NRecon program and analyzed using Skyscan CTAn software. Analysis of trabecular bone at the left distal femoral metaphysis focused on a region

of interest (ROI) extending 1 mm proximally from the proximal tip of the primary spongiosa. The ROI was selected adjacent to the endocortical surface using a freehand drawing tool at five to seven different levels. Auto-interpolation between these levels produced the total ROI for all frames selected.

Raman spectroscopy spectra

The bones and claws were assessed using Raman spectroscopy at Queen's University Belfast (Belfast, UK).

Sample analysis

Raman spectra were recorded in a grid pattern on bone and claw samples using a 160mW Avalon Instrument RamanStation R1 (Avalon Instruments, Belfast, UK) at excitation wavelength 785 nm. The samples were exposed to the laser beam for 18 seconds for the bones and 15 seconds for the claws with 0.25 mm distance between the laser points. A total of 196 and 45 spectra were collected on each bone and claw sample, respectively. As the protein concentration is much lower in bone than the claw, the bone measurements were completed in triplicate. The analyst was blinded to sample treatments throughout data acquisition and data processing.

Spectral Data analysis

The acquired Raman data was processed using Matlab 2013a (Mathworks, Cambridge UK) and Labspec 6 (Horiba UK Ltd, Stanmore, UK) software. Cosmic rays were manually corrected by comparing each spectrum in the dataset with the spectra adjacent to it and identifying any sharp features (<3 pixels, >3x SNR) that occurred in only one spectrum. The data from the Sprague-Dawley animals were used to develop models for processing and analysing the Raman spectra. This included building a baseline correction model using SVD-based background correction [29,30]. All the spectra were truncated to remove peak-less regions, intensity normalised (mean intensity of spectrum), mean centred and analysed using principle component analysis

(PCA) as previously described[24]. The PCA scores for components which exhibited a significant difference between the baseline and ovariectomised groups were put into a linear discriminant analysis, along with the normalised mean centred Raman data. The resulting discriminant scores were used to calculate sensitivity, specificity and area under the curve (AUC) performance characteristics. The processing algorithms and linear discriminant analysis (LDA) model developed on the claw data acquired from the Sprague-Dawley animals was tested on the data acquired from the Wistar rat claws to determine the transferability of the model to new samples and new populations. The Wistar group was used as a validation set, with sensitivity, specificity and AUC calculated for comparison with the Sprague-Dawley animals. The same processing algorithms and LDA model was applied to the sham ovariectomy within the Sprague-Dawley set to determine its impact on collagen and keratin. To obtain partial subtraction average normalized bone and claw spectra for detailed evaluation, the average spectrum from each group was normalised to the mean intensity of the Sprague-Dawley bone or claw spectra, then partially subtracted from the sum of all the bone or claw spectra until just before any negative features appeared in the result.

Sample size calculation

The sample size for the ovariectomy experiments was chosen to provide at least 80% power to detect a 1.8 standard difference (i.e. an effect size of ~1.8) in different micro-CT based variables between baseline, sham-operated and OVX groups. Post hoc (retrospective) power analyses showed that the effect size achieved for BV/TV was more than double (approximately 4) and the achieved power for detecting a difference in BV/TV between sham-operated and OVX groups was 100%.

Micro-CT Statistical analysis

Statistical analyses were performed using IBM (Armonk,NY) SPSS Statistics, version 19. Significant differences between groups (baseline, sham-operated and OVX) were assessed

using one-way analysis of variance (ANOVA) followed by Tukey HSD post hoc test. Power calculations were performed using G*Power software, version 3.1.9.2 (Heinrich Heine University Düsseldorf, Germany)

Results

Effects of ovariectomy on body and uterine weight

Body weight is an important determinant of bone mass and oestrogen deficiency is often associated with a significant increase in body weight [31]. As shown in Figure 1A, body weight significantly increased in Sprague-Dawley after ovariectomy. In contrast, uterine weight fell significantly after ovariectomy (data not shown), indicative of the successful removal of ovaries.

Effects of ovariectomy on bone architecture

Detailed microCT analysis confirmed that ovariectomised rats had significantly lower trabecular bone volume (Figure 1B) and this was accompanied by a significant reduction in trabecular number (Figure 1C). Ovariectomy also caused a significant increase in trabecular separation (Figure 1D) and a decrease in trabecular connectivity, indicated by the increased trabecular patter factor (Figure 1E). No significant changes were observed in trabecular thickness after ovariectomy (Figure 1F). Figure 1 (panel G) shows representative microCT images from the trabecular bone of the distal femoral metaphysis of Baseline (day zero), ovariectomised (OVX) and sham-operated Sprague-Dawley rats.

Raman spectrum of bone and claw tissue compared to standards

The average Raman spectra for Sprague-Dawley bone samples were compared to the corresponding claw samples from the same model shown in Figure 2A (I & III). For comparison, hydroxyapatite mineral, collagen and keratin standard were also included (Figure 2A II, IV &V respectively). A summary of the main peaks, their wavenumber shifts, band assignments and whether they are due to mineral, collagen or keratin are listed in Table 2. The

Raman spectrum of bone is dominated by phosphate bands similar to those of the hydroxyapatite at the lower wavenumber, while at higher wavenumber the spectrum is comprised primarily of protein-like features. Collagen can be distinguished from keratin by the presence of a strong peak due to hydroxyproline (no.7) and the absence of a distinct band for tyrosine and tryptophan peak (no. 21). Despite the mineral peaks in close proximity, the hydroxyproline peaks are identifiable in the bone spectrum, while there is no evidence of the tyrosine and tryptophan peak (no. 21).

Evaluation of spectral differences between bone and claw treatment groups

To evaluate what impact ovariectomy is having on the structure of the bone and claw compared to their respective baseline and sham OVX treatment groups, detailed analysis of the spectra was performed. The spectra of the bone and claw were scaled to the mean intensity of the spectrum for subtraction and the subtraction spectra are presented for comparison in Figures 2B and C. The bone spectra show sham and OVX treatment groups have an elevated band at peak no. 12, which is indicative of carbonate deposition within the hydroxyapatite matrix. Comparison between baseline, sham-OVX and OVX clearly indicates OVX treatment affects both the mineral and collagen matrix phases of the bone. OVX decreased the mineral bands indicated by the peaks at lower Raman shift at peak no. 1 and 3, and increased collagen bands, indicated by stronger peaks at Raman shifts at peak no. 20 and 22-24 compared to control. In the claw Raman signatures, changes to keratin secondary structure were observed; compared to baseline, OVX reduced β-sheet content (peak no. 24) and resulted in an altered α-helical conformation (peak shift from peak no. 22 in baseline to peak no. 23 in OVX group). Interestingly, the Raman spectral signatures for the bone and claw sham-OVX groups indicate sham OVX is subtly altering the structure of proteins in both tissues, but at a much lower rate than the OVX. The bone sham-OVX spectra showed a reduction in the overall protein content (peak no. 13-24) compared to baseline.

Discrimination between healthy and osteoporotic tissue using a LDA model

In this study, using the data acquired from bone and claw spectra from an osteoporotic model, an LDA model was created in an attempt to discriminate between healthy and osteoporotic bone and claw tissue. Figure 2 (panel D) shows the Sprague-Dawley bone discriminant function (A) calculated from the LDA modelled on OVX against baseline group, and for comparison the Sprague-Dawley claw discriminant function (B) calculated from the LDA modelled on the same treatment groups. The discriminant function highlights the variance between the treatment groups in both tissues. The prominent positive features are representative of the baseline (healthy state), whilst the prominent negative features illustrate the changes in the tissues induced by ovariectomy (osteoporotic state). The prominent positive peaks in the mineral phase of the bone discriminant function (left side of dotted line) include phosphate peaks, no. 1, 3 and 9 in the positive direction, while the carbonate peak (no.12) is a prominent negative peak. For comparison between the protein content of both tissues, the positive and negative peaks in the region right of the dotted line are highlighted. The prominent negative peaks shown in the bone collagen region of the discriminant function include C-H bone peaks (no 18 and 20) and amide I random peak (no. 23), and these same peaks were negative in the claw keratin discriminant function. Furthermore, the main positive peaks in the claw discriminant function, including amide I α-helix and β-sheet peaks (no. 23 and 24 respectively), were also local maxima in the bone discriminant function. The fact that these local areas of variance, from two different tissues, were the same suggests that ovariectomy is altering the structure of collagen and keratin in a similar manner.

Figure 3A shows the Sprague-Dawley bone sample LDA results modelled on the OVX group against baseline group and projected onto the sham OVX treatment group. The LDA classified the baseline group as significantly different compared to OVX, whilst the sham OVX group was classified as not significantly different. Moreover, the OVX group was significantly

different to the baseline and sham OVX groups. To give an indication of how appropriate this model is for determining differences and similarities in bone from health and osteoporotic rat tissue using Raman spectra, the sensitivity, specificity and AUC values were calculated from the derived LDA (Table 3); this model gave 89% sensitivity, 91% specificity and an area under the curve (AUC) of 94%.

The claws showed similar levels of performance to the bone tissue. The LDA for the Sprague-Dawley rat claws (Figure 3B) classified the baseline group as significantly different compared to all of the other treatment groups, with OVX being the most significant, while OVX is significantly different from baseline and sham OVX. The Wistar rats showed no significant difference between the control and ovariectomised rats at the early stages of treatment (≤8 weeks), but after the 12 week delay the ovariectomised rats had a significantly lower score than the control rats and also than the rats sacrificed at a younger age (Figure 3C). The Sprague-Dawley calibration set yielded a model with a sensitivity of 89% and a sensitivity of 82%, and AUC of 92%. The Wistar rat data used as validation of the model achieved a sensitivity of 92% and a specificity of 85%, while the AUC was 94%.

Discussion

Ageing is associated with many degenerative processes, including the weakening of bone, leading to increased susceptibility to fracture, even in the absence of significant trauma. The rat ovariectomy model is a standard model to study postmenopausal osteoporosis in pre-clinical trials [32]. Ovariectomised rats display similar stages of osteoporosis as in humans [33], and the model allows for investigation of changes occurring against a more uniform population, using younger animals (minimising effect of different rates of ageing) in a highly controlled environment. In this study, we analysed the impact of ovariectomy on bone collagen and claw keratin protein structure in ovariectomised rats using Raman spectroscopy. Collagen and

keratin have similar structures and properties [34], and in this study we showed that these proteins have similar Raman signatures in the mineral-free region.

Formation of collagen fibres in bone involves a series of complex post-translational modifications including hydroxylation of proline and lysine, glycosylation of hydroxylysine and generation of collagen crosslinks that are often associated with bone maturation [35]. Due to the interrelationship with mineralization, it would be expected that any change to collagen structure could alter collagen fibre organization and orientation and thus the mineral to collagen ratio, all of which help regulate bone strength, flexibility and fragility [35]. Previous studies have indicated that oestrogen deficiency leads to an increased turnover of the bone collagen matrix with an imbalance in favour of resorption over formation [35]. This increased rate of collagen synthesis generates abnormalities in post-translational modifications in collagen, including over-hydroxylation of lysine residues and over-glycosylation of hydroxylysine, leading to weakened collagen fibres with fewer crosslinks that affects mineralization of the fibre [36]. Using Raman spectroscopy, we showed that ovariectomy in adult rats decreased mineral to collagen ratio compared to baseline. This result agrees with previous findings [33,37] and that shows ovariectomy increases the protein content in the bone relative to the mineral content in the bone spectra.

Keratin is a key structural protein that provides cells and tissues with resilience to withstand mechanical and chemical stress [38–41]. Previous structural Raman spectroscopy analysis revealed Keratin's resilience to be due to its highly ordered structure, mostly in the α-helical conformation, with a high degree of protein folding and disulphide bond formation [42]. Thus, similar to collagen, keratin's properties most likely depend on coherent organisation and disruption of the secondary or tertiary structure of the protein would impact its ability to perform its functions. Indeed, studies by Farran *et al.* show fingernails' mechanical properties change under different conditions and this was hypothesised to occur via altered matrix

flexibility caused by breakdown of disulphide bonding [43]. Evaluation of the claw Raman spectral information in this study showed substantial changes to the secondary and tertiary structure of claw keratin upon ovariectomy. The position of the amide bands for α-helices is sensitive to the tertiary structure, with α-helices in globular proteins giving amide I bands at a higher wavenumber position than α-helices in fibrous proteins. Upon ovariectomy the Raman band corresponding to α-helices is shifted to a higher position reflecting a change in tertiary structure that suggests ovariectomy is associated with a reduction in fibrous structure and an increase in globular structure. The tertiary structure of collagen is also being altered by ovariectomy in a similar manner. Compared to baseline, ovariectomy shows an increase in amide I collagen content, particularly in the globular structure as signified by a large increase in amide I peak at a higher wavenumber position indicative of random structure (peak no. 24). Similar changes (elevated intensity around 1660 cm^{-1} and reduced intensity at 1685 cm^{-1}) in the amide I region from collagen of bone for ovariectomised rats has been reported by Orkoula et al [44]. Keratin in claws and nails is arranged in closely fitting fibrous strands. In this study, our data suggest that the rigid order to claw keratin fibres in ovariectomised rats was disrupted leading to a less organized keratin structure with more flexibility. Whilst these keratin changes are occurring upon ovariectomy, our results also suggest bone collagen structure is becoming less organised, which may impact on the organization and orientation of collagen fibres and thus affect mineral deposition; all of which are important in the maintenance of bone strength, toughness and fragility.

The model algorithm generated in this study was able to significantly distinguish the baseline and sham-ovariectomised groups from the ovariectomised group in bone and claw tissues. It should be noted that the animals that underwent sham-ovariectomy did show altered Raman signatures compared to both baseline and ovariectomy, but these changes are independent of those associated with the true ovariectomy as the LDA models did not classify the sham as

significantly different to baseline. As control animals were not sacrificed at the later age it is not possible to identify if the changes in the sham ovatiectomy are a results of natural aging compared to the baseline animals or if it could be attributed to changes induced by the body responding to the sham operation. The model illustrates that adult rats which have undergone ovariectomy have measurable differences in chemical and physical properties of the bone and claw compared to those from healthy untreated and sham rats (baseline and control models). Moreover, high sensitivity, specificity and AUC values calculated in this statistical model for the bone tissue imply that this is a suitable model for studying changes in bone collagen in relation to bone health.

In this study we also assessed whether the statistical method generated for the claws is transferable by testing the Raman derived clinical models on a second independent set of animals. The Wistar rat claw model was independent from the Sprague-Dawley claw model as they were using different species of rat and were designed and carried out in different centres. Utilising claw Raman data generated from an independent study (Wistar model) allowed for testing of the algorithm. The algorithm did not classify the Wistar claw control and ovariectomised groups as different over shorter treatment durations; however these groups were classified as significantly different at the longer treatment duration. This agrees with the differences observed in the Sprague-Dawley claw model as the treatment duration was 11 weeks. Applying the Wistar claw data as a prediction set to the Sprague-Dawley claw data (training set) shows comparable sensitivity, specificity and AUC values indicating this model is stable when applied to new populations and allows the use of keratin as a surrogate marker of bone health. These findings indicate the model has potential for evaluating differences between healthy and osteoporotic bone and claw tissues. Although the classification model for the bone tissue was not validated within this study the performance of Raman spectroscopic methods for analysing bone tissue is well established in independent studies[45–49].

In summary, interpretation of Raman signatures reveals that oestrogen deficiency in ovariectomised adult rats mediates changes within both bone and claw tissue. The ovariectomy-induced changes in the protein phase of both tissues are similar. Both proteins have a less ordered structure in the osteoporotic model compared to baseline, which indicate that the post-ovariectomy changes induce a greater degree of structural flexibility within collagen and keratin. It is likely that the less ordered collagen will impact on mineral deposition and thus fragility risk. Whilst, these collagen changes are occurring in the bone, our results suggest similar changes to keratin structure are happening concurrently. Thus, we provide evidence suggesting there is significant potential in using keratin as a surrogate marker for bone health deterioration.

Acknowledgements

Intertrade Ireland for part-funding MCC.

Conflict of interest

Crescent Diagnostics Ltd funded the work carried out by MCC, JRB, (OD), NMC, MT and SHR. AI and AS declare no conflict of interest.

References

1. WHO. *Assessment of Fracture Risk and Its Application to Screening for Postmenopausal Osteoporosis: Report of a WHO Study Group. Tech Rep Ser; 1994:843*. Geneva; 1994. http://apps.who.int//iris/handle/10665/39142.
2. Gallagher JC, Goldgar D, Moy A. Total bone calcium in normal women: Effect of age and menopause status. *J Bone Miner Res*. 2009;2(6):491-496. doi:10.1002/jbmr.5650020605.
3. EASTELL R, DELMAS PD, HODGSON SF, ERIKSEN EF, MANN KG, RIGGS BL. Bone Formation Rate in Older Normal Women: Concurrent Assessment with Bone

Histomorphometry, Calcium Kinetics, and Biochemical Markers*. *J Clin Endocrinol Metab*. 1988;67(4):741-748. doi:10.1210/jcem-67-4-741.

4. Heaney RP. Estrogen-calcium interactions in the postmenopause: a quantitative description. *Bone Miner*. 1990;11(1):67-84. doi:10.1016/0169-6009(90)90016-9.

5. Nordin BE, Need AG, Bridges A, Horowitz M. Relative contributions of years since menopause, age, and weight to vertebral density in postmenopausal women. *J Clin Endocrinol Metab*. 1992;74(1):20-23. doi:10.1210/jcem.74.1.1727821.

6. Wood AJJ, Riggs BL, Melton LJ. The Prevention and Treatment of Osteoporosis. *N Engl J Med*. 1992;327(9):620-627. doi:10.1056/NEJM199208273270908.

7. Heaney RP, Recker RR, Saville PD. Menopausal changes in bone remodeling. *J Lab Clin Med*. 1978;92(6):964-970. http://www.ncbi.nlm.nih.gov/pubmed/739174. Accessed May 15, 2017.

8. Balena R, Toolan BC, Shea M, et al. The effects of 2-year treatment with the aminobisphosphonate alendronate on bone metabolism, bone histomorphometry, and bone strength in ovariectomized nonhuman primates. *J Clin Invest*. 1993;92(6):2577-2586. doi:10.1172/JCI116872.

9. Poli V, Balena R, Fattori E, et al. Interleukin-6 deficient mice are protected from bone loss caused by estrogen depletion. *EMBO J*. 1994;13(5):1189-1196. http://www.ncbi.nlm.nih.gov/pubmed/8131749. Accessed May 15, 2017.

10. Marshall D, Johnell O, Wedel H. Meta-analysis of how well measures of bone mineral density predict occurrence of osteoporotic fractures. *BMJ*. 1996;312(7041). http://www.bmj.com/content/312/7041/1254?linkType=FULL&resid=312/7041/1254&journalCode=bmj. Accessed May 15, 2017.

11. Kanis JA, Melton LJ, Christiansen C, Johnston CC, Khaltaev N. The diagnosis of osteoporosis. *J Bone Miner Res*. 2009;9(8):1137-1141. doi:10.1002/jbmr.5650090802.

12. Odvina C V., Wergedal JE, Libanati CR, Schulz EE, Baylink DJ. Relationship between trabecular vertebral body density and fractures: A quantitative definition of spinal osteoporosis. *Metabolism*. 1988;37(3):221-228. doi:10.1016/0026-0495(88)90099-6.

13. Mazess RB. Bone density in diagnosis of osteoporosis: Thresholds and breakpoints. *Calcif Tissue Int*. 1987;41(3):117-118. doi:10.1007/BF02563789.

14. Ross PD, Wasnich RD, Vogel JM. Detection of prefracture spinal osteoporosis using bone mineral absorptiometry. *J Bone Miner Res*. 2009;3(1):1-11. doi:10.1002/jbmr.5650030103.

15. Boskey AL. Bone composition: relationship to bone fragility and antiosteoporotic drug effects. *Bonekey Rep*. 2013;2. doi:10.1038/bonekey.2013.181.

16. Bailey A, Wotton S, Sims T, Thompson P. Post-translational modifications in the collagen of human osteoporotic femoral head. *Biochem Biophys Res Commun*. 1992;185(3):801-805. doi:10.1016/0006-291X(92)91697-O.

17. Saito M, Fujii K, Soshi S, Tanaka T. Reductions in degree of mineralization and enzymatic collagen cross-links and increases in glycation-induced pentosidine in the femoral neck cortex in cases of femoral neck fracture. *Osteoporos Int*. 2006;17(7):986-995. doi:10.1007/s00198-006-0087-0.

18. Kovach I, Agrawal C, Richards-Kortum R, Wang X, Athanasiou K. Laser-induced autofluorescence and fracture toughness of baboon cortical bone. In: *Proceedings of the 43th Annual Meeting of the Orthopaedic Society*. San Francisco; 1997:22:37.

19. Wang X, Shen X, Li X, Mauli Agrawal C. Age-related changes in the collagen network and toughness of bone. *Bone*. 2002;31(1):1-7. doi:10.1016/S8756-3282(01)00697-4.

20. McCreadie BR, Morris MD, Chen T, et al. Bone tissue compositional differences in women with and without osteoporotic fracture. *Bone*. 2006;39(6):1190-1195. doi:10.1016/j.bone.2006.06.008.

21. Pillay I, Lyons D, German MJ, et al. The use of fingernails as a means of assessing bone health: a pilot study. *J Womens Health (Larchmt)*. 2005;14(4):339-344. doi:10.1089/jwh.2005.14.339.

22. Moran P, Towler MR, Chowdhury S, et al. Preliminary work on the development of a novel detection method for osteoporosis. *J Mater Sci Mater Med*. 2007;18(6):969-974. doi:10.1007/s10856-006-0037-6.

23. Towler MR, Wren A, Rushe N, Saunders J, Cummins NM, Jakeman PM. Raman spectroscopy of the human nail: A potential tool for evaluating bone health? *J Mater Sci Mater Med*. 2007;18(5):759-763. doi:10.1007/s10856-006-0018-9.

24. Beattie JR, Cummins NM, Caraher MC, et al. Assessing fracture risk in post-menopausal women by Raman spectroscopic analysis of fingernail clippings. *Clin Med Insights (Arthritis Musculoskelet Disord*. 2016;In Press.

25. Beattie JR, Feskanich D, Caraher MC, Towler MR. A preliminary evaluation of the ability of keratotic tissue to act as a prognostic indicator of fracture risk. *J Bone Miner Res*. 2017;Submitted.

26. Beattie JR, Caraher MC, Cummins NM, et al. Raman spectral variation for human fingernails of postmenopausal women is dependent on fracture risk and osteoporosis status. *J Raman Spectrosc*. 2017. doi:10.1002/jrs.5123.

27. Sophocleous A, Idris AI. Rodent models of osteoporosis. *Bonekey Rep*. 2014;3. doi:10.1038/bonekey.2014.109.

28. Campbell GM, Sophocleous A. Quantitative analysis of bone and soft tissue by micro-computed tomography: applications to ex vivo and in vivo studies. *Bonekey Rep*. 2014;3. doi:10.1038/bonekey.2014.59.

29. Beattie JR, McGarvey JJ. Estimation of signal backgrounds on multivariate loadings improves model generation in face of complex variation in backgrounds and

constituents. *J Raman Spectrosc*. 2013;44(2):329-338. doi:10.1002/jrs.4178.

30. Beattie JR. Optimising reproducibility in low quality signals without smoothing; An alternative paradigm for signal processing. *J Raman Spectrosc*. 2011;42(6):1419-1427. doi:10.1002/jrs.2851.

31. Mueller K, Hsiao S. Estrus- and ovariectomy-induced body weight changes: Evidence for two estrogenic mechanisms. *J Comp Physiol Psychol*. 1980;94(6):1126-1134. doi:10.1037/h0077746.

32. Lelovas PP, Xanthos TT, Thoma SE, Lyritis GP, Dontas IA. The Laboratory Rat as an Animal Model for Osteoporosis Research. http://www.ingentaconnect.com/content/aalas/cm/2008/00000058/00000005/art00001. Accessed May 15, 2017.

33. WRONSKI TJ, CINTRON M, DOHERTY AL, DANN LM. Estrogen Treatment Prevents Osteopenia and Depresses Bone Turnover in Ovariectomized Rats*. *Endocrinology*. 1988;123(2):681-686. doi:10.1210/endo-123-2-681.

34. Colla F, Brühlmann P, Panizzon R, Michel BA. [Osteopoikilosis--skin and joint manifestations]. *Z Rheumatol*. 1995;54(2):123-127. http://www.ncbi.nlm.nih.gov/pubmed/7793159. Accessed May 15, 2017.

35. Viguet-Carrin S, Garnero P, Delmas PD. The role of collagen in bone strength. *Osteoporos Int*. 2006;17(3):319-336. doi:10.1007/s00198-005-2035-9.

36. Bailey AJ, Wotton SF, Sims TJ, Thompson PW. Biochemical changes in the collagen of human osteoporotic bone matrix. *Connect Tissue Res*. 1993;29(2):119-132. doi:10.3109/03008209309014239.

37. Wronski TJ, Lowry PL, Walsh CC, Ignaszewski LA. Skeletal alterations in ovariectomized rats. *Calcif Tissue Int*. 1985;37(3):324-328. doi:10.1007/BF02554882.

38. Fuchs E, Cleveland DW. A structural scaffolding of intermediate filaments in health and

disease. *Science (80-).* 1998;279(5350):514-519. doi:10.1126/science.279.5350.514.

39. Seltmann K, Fritsch AW, Käs JA, Magin TM. Keratins significantly contribute to cell stiffness and impact invasive behavior. *Proc Natl Acad Sci U S A*. 2013;110(46):18507-18512. doi:10.1073/pnas.1310493110.

40. Ramms L, Fabris G, Windoffer R, et al. Keratins as the main component for the mechanical integrity of keratinocytes. *Proc Natl Acad Sci U S A*. 2013;110(46):18513-18518. doi:10.1073/pnas.1313491110.

41. Farren L, Shayler S, Ennos AR. The fracture properties and mechanical design of human fingernails. *J Exp Biol*. 2004;207(5). http://jeb.biologists.org/content/207/5/735.short. Accessed May 15, 2017.

42. Gniadecka M, Nielsen OF, Christensen DH, Wulf HC. Structure of Water, Proteins, and Lipids in Intact Human Skin, Hair, and Nail. *J Invest Dermatol*. 1998;110(4):393-398. doi:10.1046/j.1523-1747.1998.00146.x.

43. Farran L, Ennos AR, Eichhorn SJ. The effect of humidity on the fracture properties of human fingernails. *J Exp Biol*. 2008;211(23). http://jeb.biologists.org/content/211/23/3677.short. Accessed May 15, 2017.

44. Orkoula MG, Vardaki MZ, Kontoyannis CG. Study of bone matrix changes induced by osteoporosis in rat tibia using Raman spectroscopy. *Vib Spectrosc*. 2012;63:404-408. doi:10.1016/j.vibspec.2012.09.016.

45. Draper ER, Morris MD, Camacho NP, et al. Novel Assessment of Bone Using Time-Resolved Transcutaneous Raman Spectroscopy. *J Bone Miner Res*. 2005;20(11):1968-1972. doi:10.1359/JBMR.050710.

46. Morris MD, Mandair GS. Raman Assessment of Bone Quality. *Clin Orthop Relat Res*. 2011;469(8):2160-2169. doi:10.1007/s11999-010-1692-y.

47. Shen J, Fan L, Yang J, Shen AG, Hu JM. A longitudinal Raman microspectroscopic study

of osteoporosis induced by spinal cord injury. *Osteoporos Int*. 2010;21(1):81-87. doi:10.1007/s00198-009-0949-3.

48. Demers J-LH, Esmonde-White FWL, Esmonde-White KA, Morris MD, Pogue BW. Next-generation Raman tomography instrument for non-invasive in vivo bone imaging. *Biomed Opt Express*. 2015;6(3):793. doi:10.1364/BOE.6.000793.

49. Mandair GS, Esmonde-White FWL, Akhter MP, et al. Potential of Raman spectroscopy for evaluation of bone quality in osteoporosis patients: results of a prospective study. In: Kollias N, Choi B, Zeng H, et al., eds. International Society for Optics and Photonics; 2010:754846. doi:10.1117/12.842515.

Figure legends

Figure 1. Effects of ovariectomy model in Sprague-Dawley rats. **(**A) Body weight (g) in ovariectomised and sham-operated Sprague-Dawley rats. (B-F) MicroCT analysis of trabecular bone at the distal femoral metaphysis (B, trabecular bone volume, BV/TV, %; C, trabecular number, Tb.N, μm; D, trabecular separation, Tb.Sp, μm; E, trabecular pattern factor, Tb.Pf, 1/μm; F, trabecular thickness, Tb.Th, μm;). The values shown are mean ± sem. *$p < 0.05$ vs. Sham by one-way analysis of variance (ANOVA). (G) Representative microCT images from

the trabecular bone of the distal femoral metaphysis of Baseline (day zero), ovariectomised (OVX) and sham-operated Sprague-Dawley rats.

Figure 2. (A) Average normalised Raman spectra of Sprague-Dawley bone (i) and claw (iii) samples. The average spectra for the bone and claw models are compared to hydroxyapatite (ii), collagen (iv) and keratin (v). (B-C) Subtraction spectra for average (i) ovariectomy and (ii) sham ovariectomy minus baseline from bone (B) and claw (C) samples. Selected Raman bands are labelled against table 2 with the corresponding wavelength in brackets. (D) The discriminant function for Sprague-Dawley bone (i) and claw (ii) samples as determined by the linear discriminant analysis (LDA) modeled on the respective ovariectomised (OVX) group against baseline group and projected onto the other treatment groups. The mineral peaks (350-1100cm^{-1}) are labeled in the bone spectra including peak number and wavenumber. While the corresponding protein peaks (1100-1800cm^{-1}) in the bone collagen and claw keratin are indicated including peak number and wavenumber.

Figure 3. Mean scores for ovariectomy discriminant models (built on OVX vs baseline, applied to sham) based on A) Sprague-Dawley bone tissue B) Sprague-Dawley claw tissue and C) model derived from Sprague Dawley claw tissue applied to Wistar rat claw tissue. The Wistar animals were split into those culled within 8 and 12 or more weeks of study start, with the longer growth time being used as the validation set for the model. Error bars represent 95% confidence interval. Significance between Control and each treatment group (indicated by * and solid lines), and between OVX and each treatment group (indicated by * and dotted lines) was measured. ** $p<0.01$, ***$p< 0.001$.

Tables

Table 1. Wistar study design.

Group	Surgical intervention	Duration (weeks)	(n)
1	None	0	4
2	None	2	6
3	OVX	2	6
4	None	4	6
5	OVX	4	6
6	None	8	6
7	OVX	8	6
8	None	12	6
9	OVX	12	6
10	None	20	7
11	OVX	20	6

The table lists the number of different groups according to duration and the number of samples in each group. Ovariectomy (OVX).

Table 2. Bone and Claw Raman spectroscopy Band Assignments.

Peak No.	Raman Shift (cm^{-1})	Assignment	Keratin/Collagen/Mineral	References
1	430	PO_4^{3-} $\nu_{2\ AS}$	Mineral	[28]
2	510	Disulfide, ν (S-S)	Keratin	[22,23,29]
3	580-590	PO_4^{3-} $\nu_{4\ AS}$	Mineral	[28]
4	644	Cysteine, ν (CS)	Keratin	[23]
5	830	Tyrosine, δ (CCH) $_{OP}$	Collagen/Keratin	[29]
6	850	Tyrosine/O-P-O, δ (CCH) ring breathing	Collagen/Keratin/Mineral	[29]
7	856	Hydroxyproline	Collagen	[30]
8	936	α-helix, ν (CC)	Collagen/Keratin	[29]
9	960	PO_4^{3-} ν_1	Mineral	[30]
10	1004	Phenylalanine	Collagen/Keratin	[23,29]
11	1032	Phenylalanine	Collagen/Keratin	[29]
12	1070	CO_4^{3-} (ν)	Mineral	[30]
13	1078	Carbon backbone, ν (CC) $_{RC}$	Collagen/Keratin	[29]
14	1126	Carbon backbone, ν (CC) $_{TC}$	Collagen/Keratin	[29]
15	1206	Tyrosine and Phenylalanine, ν (C-C_6H_5)	Collagen/Keratin	[28]
16	1240	β-sheet, Amide III	Collagen/Keratin	[30]
17	1256	Random, Amide III	Collagen/Keratin	[23,29]
18	1305	α-helix, Amide III	Collagen/Keratin	[30]
19	1420	C-H bonding, δ (CH_3) deformation	Collagen/Keratin	[29]
20	1450	C-H bonding, δ (CH_2) scissoring	Collagen/Keratin	[23,29]
21	1614	Tyrosine and Tryptophan, C=C stretching	Keratin	[29]
22	1642-44	α-helix, ν (CO) amide I	Collagen/Keratin	[31]
23	1652-56	Random, ν (CO) amide I	Collagen/Keratin	[29, 31]

24	1668-75	β-sheet, ν (CO) amide I	Collagen/Keratin

The main peaks present in the bone and claw spectra are listed in numerical order including their wavenumbers, band assignments, whether they are keratin, collagen or mineral bands and band assignment references. Asymmetric stretch (AS), out of plane (γ), in plane (δ) random conformation (RC), trans conformation (TC) and stretch (ν).

Table 3. Linear discriminant analysis (LDA) was modelled on ovariectomised (OVX) group against control group and projected onto the other treatment groups in the bone samples.

	OVX vs Control	($n_{control}$)	(n_{OVX})	Sensitivity (%)	Specificity (%)	AUC (%)
Bone	**Sprague-Dawley (12 weeks)**	9	11	89	91	94
Claw	**Sprague-Dawley (12 weeks)** ***calibration model***	9	11	89	82	92
	Wistar (≥12 weeks) ***validation model***	13	12	92	85	94

The sensitivity, specificity and AUC (area under the curve) values are shown.

Figures

Figure 1.

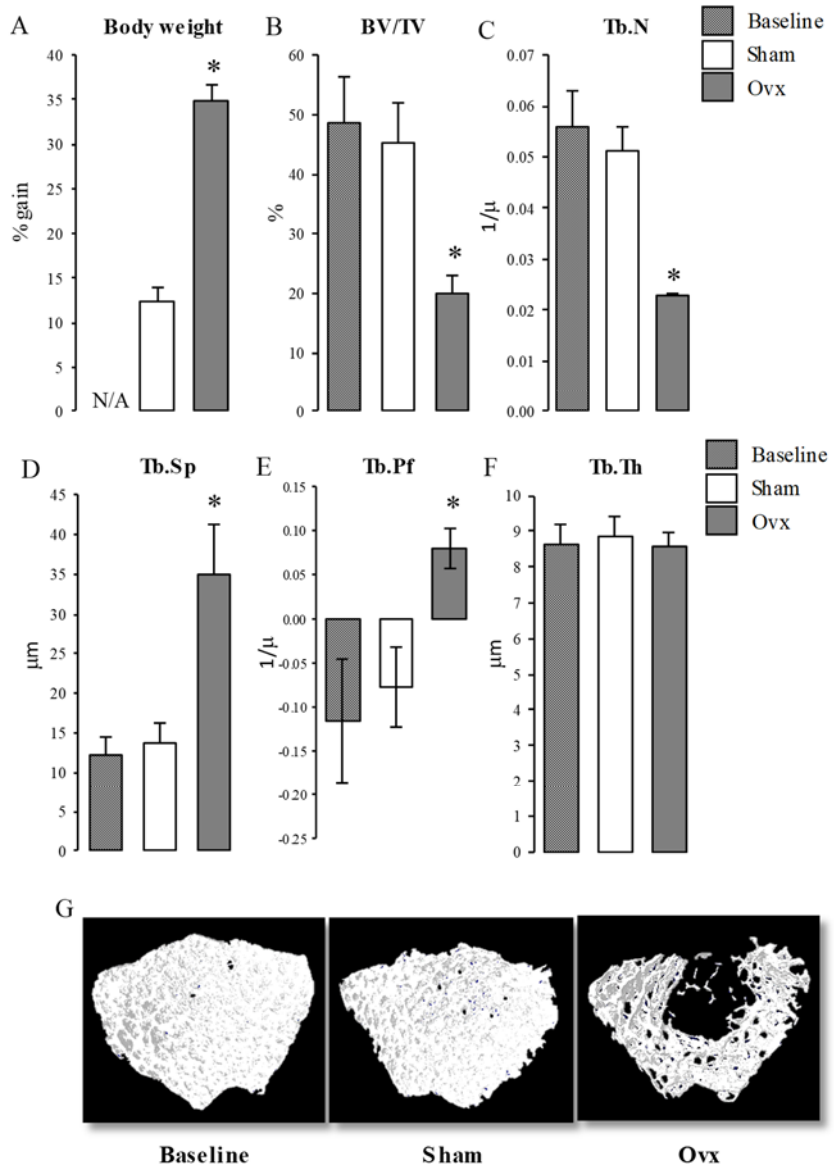

Figure 2.

Figure 2.

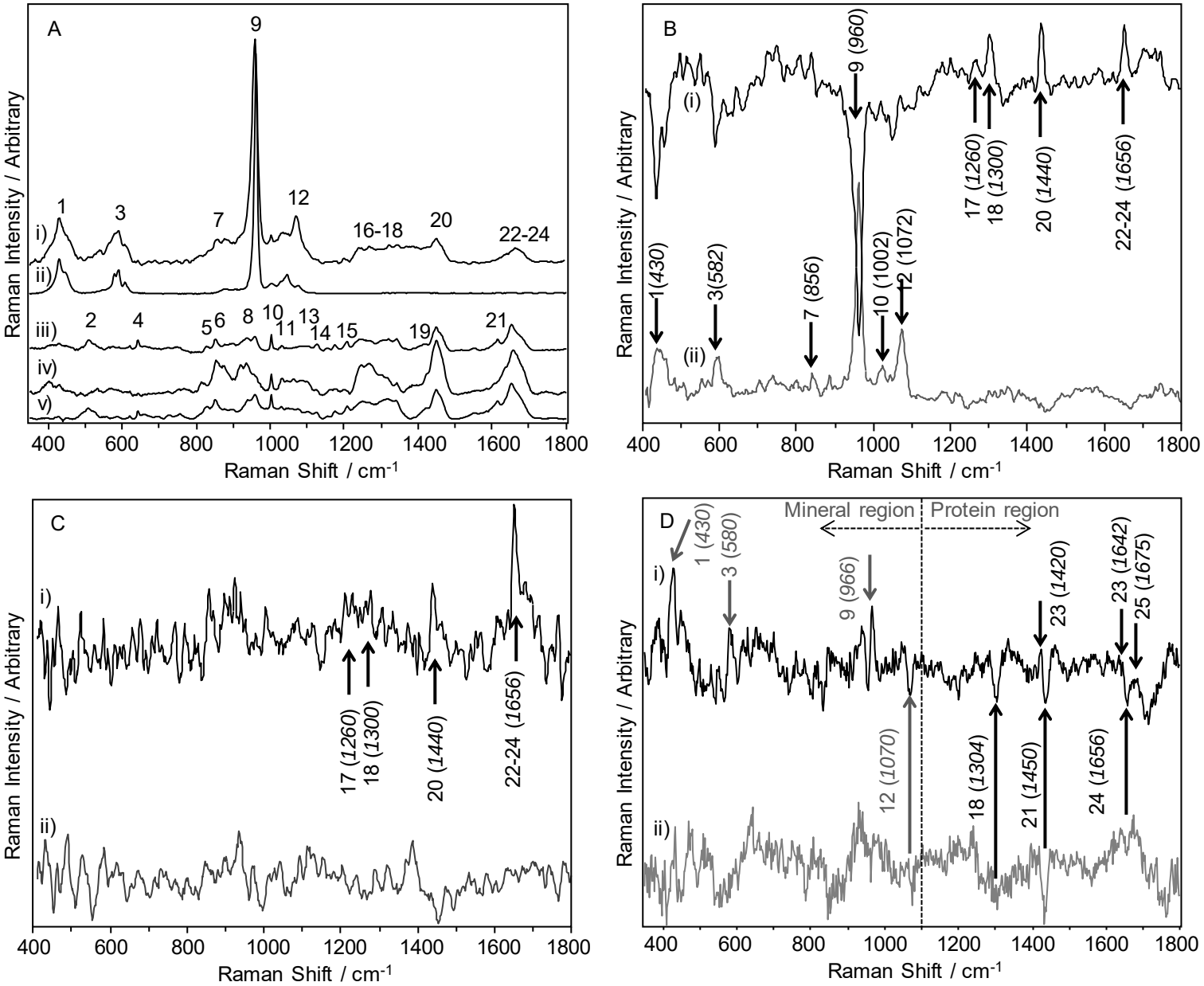
A
B
C
D
Raman Intensity / Arbitrary
Raman Shift / cm-1
i)
ii)
iii)
iv)
v)
1
2
3
4
5
6
7
8
9
10
11
12
13
14
15
16-18
19
20
21
22-24
1(430)
3(582)
7 (856)
9 (960)
10 (1002)
12 (1072)
17 (1260)
18 (1300)
20 (1440)
22-24 (1656)
Mineral region
Protein region
1 (430)
3 (580)
9 (966)
12 (1070)
18 (1304)
21 (1450)
23 (1420)
23 (1642)
24 (1656)
25 (1675)

Figure 3.

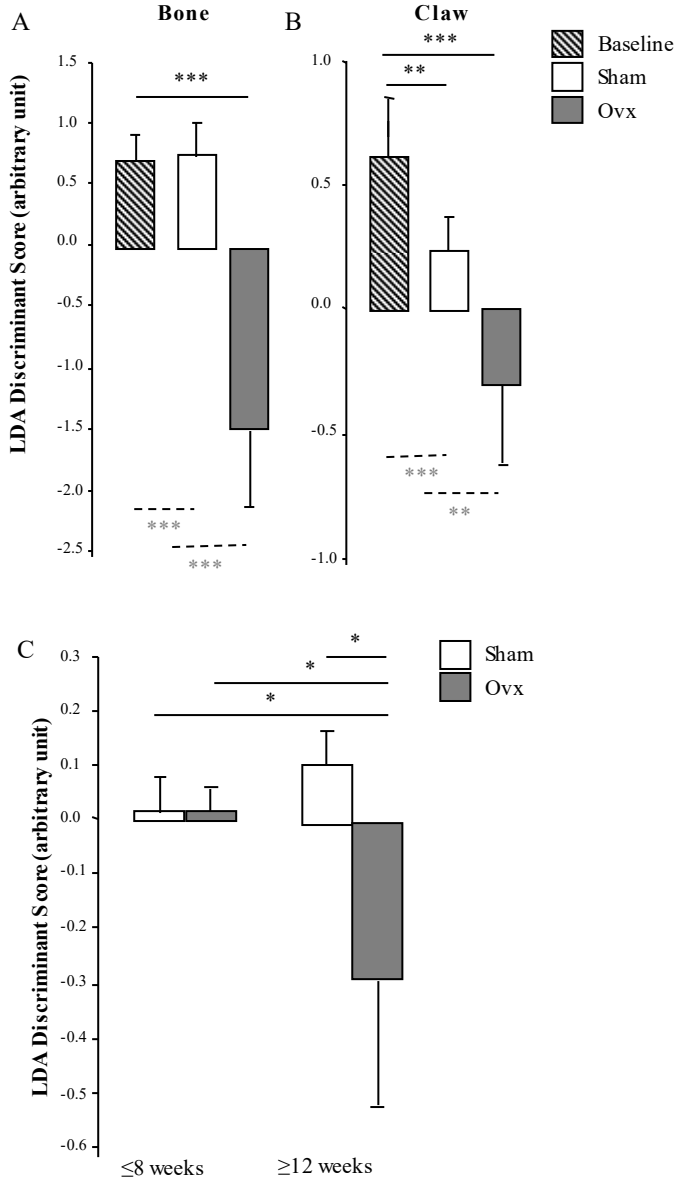
A
Bone
B
Claw
Baseline
Sham
Ovx
LDA Discriminant Score (arbitrary unit)
1.5
1.0
0.5
0.0
-0.5
-1.0
-1.5
-2.0
-2.5
***
***
***
1.0
0.5
0.0
-0.5
-1.0
***
**
***
**
C
Sham
Ovx
LDA Discriminant Score (arbitrary unit)
0.3
0.2
0.1
0.0
-0.1
-0.2
-0.3
-0.4
-0.5
-0.6
*
*
*
≤8 weeks
≥12 weeks